

## Supplementary Information

# Isolation of an Organometallic Yttrium Bismuth Cluster and Elucidation of its Electronic Structure

Elizabeth R. Pugliese, Florian Benner, Selvan Demir\*

Department of Chemistry, Michigan State University, 578 South Shaw Lane, East Lansing, Michigan 48824, USA

\*Correspondence to: [sdemir@chemistry.msu.edu](mailto:sdemir@chemistry.msu.edu) (S.D.)

# Table of Contents

<b>1.1 Experimental Methods</b>	<b>S3</b>
<b>1.2 X-ray Crystallography</b>	<b>S6</b>
Table S1. Crystal data and structural refinement of $[\text{K}(\text{THF})_4]_2[\text{Cp}^*_2\text{Y}_2\text{Bi}_6]$ ( <b>1</b> ) and $\text{Cp}^*_2\text{YPh}(\text{THF})$ ( <b>2</b> ).	<b>S6</b>
Figure S1. Structure of $[\text{Cp}^*_2\text{Y}_2\text{Bi}_6]^{2-}$ in a crystal of <b>1</b> , with thermal ellipsoids drawn at 50% probability level.	<b>S7</b>
Figure S2. Space filling model of $[\text{Cp}^*_2\text{Y}_2\text{Bi}_6]^{2-}$ in a crystal of <b>1</b> .	<b>S8</b>
Figure S3. Structure of $\text{Cp}^*_2\text{YPh}(\text{THF})$ , <b>2</b> .	<b>S9</b>
Figure S4. Crystal packing diagram of $[\text{K}(\text{THF})_4]_2[\text{Cp}^*_2\text{Y}_2\text{Bi}_6]$ ( <b>1</b> ).	<b>S10</b>
<b>1.3 DFT Calculations</b>	<b>S11</b>
Figure S5. Plots of the calculated mean deviation (MD), mean square error (MSE), root mean square error (RMSE) and mean absolute percentage error (MAPE).	<b>S11</b>
Figure S6. Plots of the calculated set of highest occupied molecular orbitals (HOMO-4 to HOMO+5) of the $[\text{Cp}^*_2\text{Y}_2\text{Bi}_6]^{2-}$ anion.	<b>S12</b>
Table S2. Results of the hybridisation/polarisation analysis of NLMOs as the % contributions of parent NBOs of <b>1</b> .	<b>S13</b>
Table S3. Results of the hybridisation/polarisation analysis of NLMOs as the % orbital contributions of <b>1</b> .	<b>S14</b>
Table S4. Results of the hybridisation/polarisation analysis of NLMOs for the Bi lone electron pairs as the % orbital contributions of <b>1</b> .	<b>S14</b>
Table S5. Results of the second order perturbation analysis of the optimised structure of the $[\text{Cp}^*_2\text{Y}_2\text{Bi}_6]^{2-}$ anion.	<b>S15</b>
Table S6. Real space values of critical points as obtained from QTAIM analysis on the $[\text{Cp}^*_2\text{Y}_2\text{Bi}_6]^{2-}$ anion.	<b>S18</b>
Figure S7. Plot of the electron localisation function (ELF) of the $[\text{Cp}^*_2\text{Y}_2\text{Bi}_6]^{2-}$ anion.	<b>S19</b>
Figure S8. Calculated nuclear-independent chemical shift (NICS) values of the $[\text{Cp}^*_2\text{Y}_2\text{Bi}_6]^{2-}$ anion with printed ghost atoms.	<b>S20</b>
Figure S9. Distance-dependent plots of the calculated NICS values for the $\text{Bi}_6^{6-}$ core without capping $(\text{Cp}^*\text{Y})^{2+}$ units.	<b>S21</b>
<b>1.4 UV-Vis spectroscopy and TDDFT calculations</b>	<b>S22</b>
Figure S10. UV-Vis absorption spectra of <b>1</b> recorded at 100 $\mu\text{mol/L}$ , 50 $\mu\text{mol/L}$ and 20 $\mu\text{mol/L}$ concentrations in THF at room temperature.	<b>S22</b>
Table S7. TDDFT-calculated transitions for the $[\text{Cp}^*_2\text{Y}_2\text{Bi}_6]^{2-}$ anion.	<b>S23</b>
<b>1.5 References</b>	<b>S26</b>

## 1.1 Experimental Methods

### General Information

The manipulations described herein were performed under an inert argon atmosphere with rigorous exclusion of air and water using Schlenk line and glovebox techniques. *N*-Hexane was dried over calcium hydride. Diethyl ether and THF were dried over a Na/K alloy. Toluene was distilled over potassium. Potassium bis(trimethylsilylamide) (KN[Si(CH<sub>3</sub>)<sub>3</sub>]<sub>2</sub>) was purchased from Sigma-Aldrich, dissolved in toluene, centrifuged, filtered, and recrystallised at -35 °C. Triphenylbismuth (BiPh<sub>3</sub>) was purchased from Sigma-Aldrich and recrystallised from hexane at -35 °C. 1,2,3,4,5-Pentamethylcyclopentadiene (HCp\*) was purchased from Sigma-Aldrich and dried over 4 Å sieves. Anhydrous yttrium chloride (YCl<sub>3</sub>) and allylmagnesium chloride (2.0 M in THF) were purchased from Sigma-Aldrich and used as received. KCp\* was synthesised by deprotonation of HCp\* with K[N(SiMe<sub>3</sub>)<sub>2</sub>].<sup>1</sup> KC<sub>8</sub>,<sup>2</sup> (HNEt<sub>3</sub>)(BPh<sub>4</sub>),<sup>3</sup> and Cp\*<sub>2</sub>Y(BPh<sub>4</sub>),<sup>4</sup> were prepared according to literature procedures. A PerkinElmer 2400 Series II CHNS/O analyser was used for CHN elemental analyses.

**[K(THF)<sub>4</sub>]<sub>2</sub>[Cp\*<sub>2</sub>Y<sub>2</sub>Bi<sub>6</sub>] (1).** In an argon filled glovebox, BiPh<sub>3</sub> (19.9 mg, 0.0451 mmol) was dissolved in 2 mL of THF and added to a 5 mL colorless solution of Cp\*<sub>2</sub>Y(BPh<sub>4</sub>) (102.0 mg, 0.1503 mmol) in THF. Subsequently, KC<sub>8</sub> (22.6 mg, 0.165 mmol) was added at once to the reaction mixture and stirred for 15 minutes at room temperature. The dark red solution was filtered to remove the black and colorless insoluble material, presumably graphite and KBPh<sub>4</sub>. The solvent was removed *in vacuo* to afford a dark solid which was washed three times with 5 mL of hexane and twice with 5 mL of toluene to remove the byproduct Cp\*<sub>2</sub>YPh(THF) (2). The remaining black solid was dissolved in 5 mL of THF and filtered to obtain a dark brown solution, which was evaporated to dryness. The solids were dissolved in 1 mL of THF. Black, block-shaped crystals, suitable for single crystal X-ray diffraction analysis were crystallised from the THF solution via vapor diffusion of hexane at -35 °C in 12% yield, based on BiPh<sub>3</sub>. Anal. Calc. for Y<sub>2</sub>Bi<sub>6</sub>C<sub>20</sub>H<sub>30</sub>K<sub>2</sub>•0.5THF: C, 14.55; H, 1.89; N, 0.0. Found. C, 14.53; H, 1.42; N, 0.36. Anal Calc. for YC<sub>30</sub>H<sub>43</sub>O: C, 70.85; H, 8.52; N, 0.0. Found. C, 70.24; H, 9.10; N, 0.14.

### X-ray Crystallography.

A black block-shaped crystal of **1**, 0.20 × 0.149 × 0.077 mm<sup>3</sup>, was mounted on a nylon loop with Paratone oil. Data were collected using a XtaLAB Synergy, Dualflex, HyPix diffractometer equipped with an Oxford Cryosystems low-temperature device, operating at T = 100.0(1) K.

Data were measured using ω scans using Mo Kα radiation (microfocus sealed X-ray tube, 50 kV, 1 mA). The total number of runs and images was based on the strategy calculation from the program CrysAlisPro (Rigaku, V1.171.41.90a, 2020). Cell parameters were retrieved using CrysAlisPro (Rigaku, V1.171.41.90a, 2020) software and refined using CrysAlisPro (Rigaku, V1.171.41.90a, 2020). Data reduction was performed using the CrysAlisPro (Rigaku, V1.171.41.90a, 2020) software, which corrects for Lorentz-polarisation. A numerical absorption correction based on Gaussian integration over a multifaceted crystal model empirical absorption

correction using spherical harmonics was implemented in the SCALE3 ABSPACK scaling algorithm.

The structure was solved in the space group  $P2_1/n$  by using dual methods with the ShelXT (Sheldrick, 2015) structure solution program.<sup>5</sup> The structure was refined by least squares using version 20189/2 of XL<sup>6</sup> incorporated in Olex2.<sup>7</sup> All non-hydrogen atoms were refined anisotropically. Hydrogen atom positions were calculated geometrically and refined using the riding model.

A colorless block-shaped crystal of **2**,  $0.48 \times 0.4 \times 0.17$  mm<sup>3</sup>, was mounted on a nylon loop with Paratone oil. Data were collected using a XtaLAB Synergy, Dualflex, HyPix diffractometer equipped with an Oxford Cryosystems low-temperature device, operating at  $T = 100.0(1)$  K.

Data were measured using  $\omega$  scans using Mo K $\alpha$  radiation (microfocus sealed X-ray tube, 50 kV, 1 mA). The total number of runs and images was based on the strategy calculation from the program CrysAlisPro (Rigaku, V1.171.41.90a, 2020). Cell parameters were retrieved using CrysAlisPro (Rigaku, V1.171.41.90a, 2020) software and refined using CrysAlisPro (Rigaku, V1.171.41.90a, 2020). Data reduction was performed using the CrysAlisPro (Rigaku, V1.171.41.90a, 2020) software, which corrects for Lorentz–polarisation. A numerical absorption correction based on Gaussian integration over a multifaceted crystal model empirical absorption correction using spherical harmonics was implemented in the SCALE3 ABSPACK scaling algorithm.

The structure was solved in the space group  $P2_1/c$  by using dual methods with the ShelXT (Sheldrick, 2015) structure solution program.<sup>5</sup> The structure was refined by least squares using version 20189/2 of XL<sup>6</sup> incorporated in Olex2.<sup>7</sup> All non-hydrogen atoms were refined anisotropically. Hydrogen atom positions were calculated geometrically and refined using the riding model.

### UV-Vis Spectroscopy.

UV-vis spectra were collected with an Agilent Cary 60 spectrophotometer at ambient temperature from 200 to 1100 nm. Samples were prepared in an argon-filled glovebox and measured in a 1 cm quartz cuvette. The spectrum is baseline corrected from a sample of dry and filtered THF.

### Computational Methods

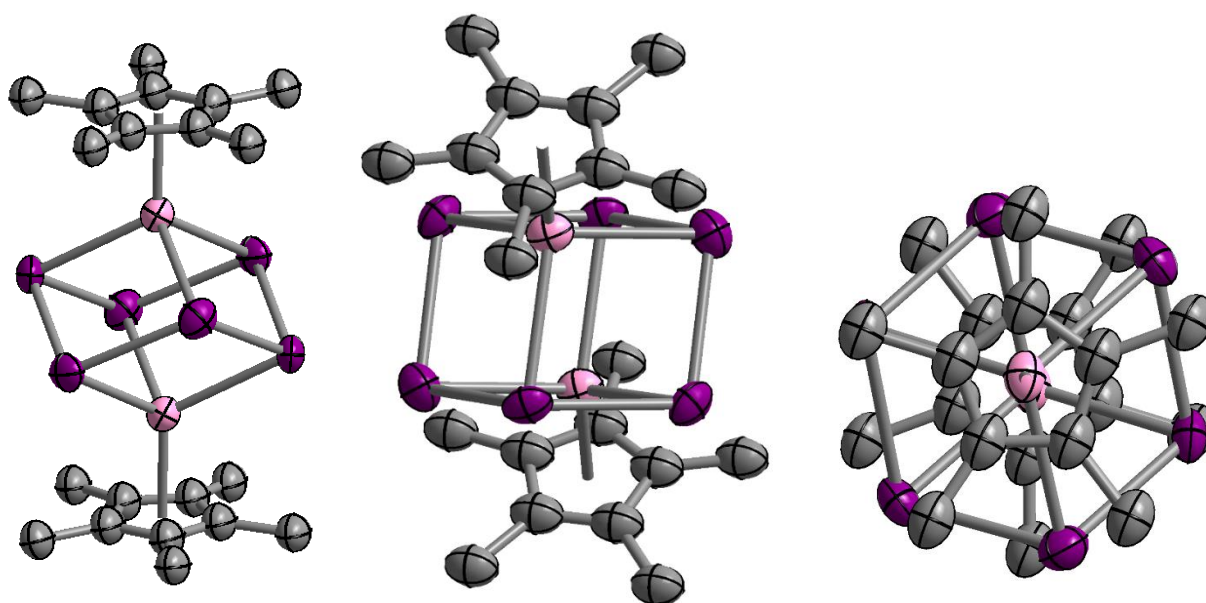
Density functional theory (DFT) calculations were carried out using the program Gaussian V16 (Rev. B01)<sup>8</sup> on the coordinates of the  $[\text{Cp}^*_2\text{Y}_2\text{Bi}_6]^{2-}$  anion as obtained from single-crystal X-ray analysis in singlet state. The geometry was successively optimised with a three step strategy: 1) 321G(C,H,Y)/def2-SVP(Bi);<sup>9,10</sup> 2) 631+G\*(C,H)/SVPD(Y,Bi);<sup>11–15</sup> 3) 631+G\*(C,H)/ECP60MDF\_VDZ(Bi)/ECP28MDF\_VDZ(Y).<sup>11–14,16,17</sup> The optimisations were carried out with the functionals TPSSSTPSS,<sup>18</sup> TPSSh,<sup>18,19</sup> B3LYP,<sup>20–23</sup> CAM-B3LYP,<sup>24</sup> BP86,<sup>25,26</sup>  $\omega$ 97xD,<sup>27</sup> PBEPBE,<sup>28,29</sup> and PBE0<sup>28–30</sup> with the fully relativistic pseudopotentials ECP28MDF and ECP60MDF on the Y<sup>17</sup> and Bi<sup>31</sup> atoms, respectively, and under consideration of the empirical dispersion correction GD3 by Grimme.<sup>32,33</sup> After all optimisations converged on level 3) of theory

and were confirmed to be minimum structures via frequency calculations (one imaginary frequency at  $\sim 10\text{ cm}^{-1}$ , associated with an in-plane rotation of the Cp\* rings was returned in all cases and could not be eliminated through additional optimisations) the metrical parameters of the obtained structures were compared with the coordinates obtained from single-crystal X-ray diffraction analysis in order to find the exchange correlation functional best-suited to describe the bonding situation in the  $[\text{Cp}^*_2\text{Y}_2\text{Bi}_6]^{2-}$  anion. Here, the PBE0 functional proved to be best-suited, as deduced by the mean deviation (MD), mean square error (MSE), root mean square error (RMSE) and mean absolute percentage error (MAPE), Figure S5. As a general note, all DFT functionals predict longer Bi–Bi and Y–Bi bonds, thereby underestimating the covalent character and/or aromatic stabilization of these bonds to some extent. Subsequently, the negative charge of the cluster was compensated by employing the polarisable conductor calculation model (CPCM, with parameters chosen for tetrahydrofuran)<sup>34,35</sup> in an additional optimisation step on the PBE0/6311+G\*(C,H)/ECP\_AVTZ(Bi,Y) level of theory. Single point calculations were carried out on the obtained structure for natural localised molecular orbital (NLMO)<sup>36</sup> with NBO6,<sup>36</sup> nucleus independent chemical shift (NICS),<sup>32</sup> quantum theory of atoms in molecules (QTAIM)<sup>37,38</sup> and electron localisation function (ELF) calculations. The latter two analyses were conducted using the program MultiWfn.<sup>39</sup> TDDFT calculations were carried out on the CPCM-optimised structure for 75 excited states for the  $[\text{Cp}^*_2\text{Y}_2\text{Bi}_6]^{2-}$  anion on the 6311+G\*(C,H)/ECP\_AVTZ(Bi,Y) level using the PBE0 functional with dispersion correction GD3 and implicit solvent model CPCM for THF. UV-vis spectra were simulated via application of a 0.1 eV Gaussian broadening using the MultiWfn program. The transitions were empirically shifted by 0.4 eV.

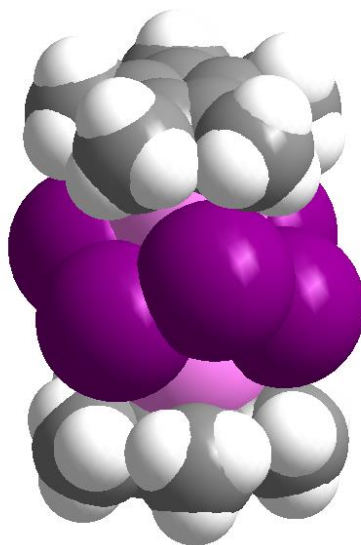
## 1.2 X-ray Crystallography

**Table S1.** Crystal data and structural refinement of [K(THF)<sub>4</sub>]<sub>2</sub>[Cp\*<sub>2</sub>Y<sub>2</sub>Bi<sub>6</sub>] (**1**) and Cp\*<sub>2</sub>YPh(THF) (**2**).

Compound	1	2
Empirical formula	C <sub>52</sub> H <sub>94</sub> Bi <sub>6</sub> K <sub>2</sub> O <sub>8</sub> Y <sub>2</sub>	C <sub>30</sub> H <sub>43</sub> OY
CCDC number	2292178	2292179
Formula weight (g mol <sup>-1</sup> )	2357.17	508.55
Temperature (K)	100.0(1)	100.0(1)
Crystal system	Monoclinic	Monoclinic
Space group	<i>P</i> 2 <sub>1</sub> / <i>n</i>	<i>P</i> 2 <sub>1</sub> / <i>c</i>
Unit Cell Dimensions	<i>a</i> = 13.3252(3) Å <i>b</i> = 16.7323(5) Å <i>c</i> = 15.4540(5) Å <i>α</i> = 90° <i>β</i> = 100.961(3)° <i>γ</i> = 90°	<i>a</i> = 9.4266(2) Å <i>b</i> = 17.1628(3) Å <i>c</i> = 16.8285(3) Å <i>α</i> = 90° <i>β</i> = 102.699(2)° <i>γ</i> = 90°
Volume (Å <sup>3</sup> )	3382.79(17)	2656.03(9)
<i>Z</i>	2	4
<i>ρ</i> <sub>calc</sub> (g cm <sup>-3</sup> )	2.314	1.272
<i>μ</i> (mm <sup>-1</sup> )	17.407	2.214
<i>F</i> (000)	2168.0	1080.0
Crystal size (mm <sup>3</sup> )	0.20 x 0.149 x 0.077	0.48 x 0.4 x 0.17
Radiation	Mo K <sub>α</sub> (λ = 0.71073)	Mo K <sub>α</sub> (λ = 0.71073)
2 $\theta$ range for data collection (°)	4.432 to 50.498	5.882 to 61.684
Reflections collected	32621	32939
Independent reflections	6102 <i>R</i> <sub>int</sub> = 0.0575	6862 <i>R</i> <sub>int</sub> = 0.0304
Data/restraints/parameters	6102/1107/611	6862/0/299
Goodness-of-fit on <i>F</i> <sup>2</sup>	1.015	1.053
Final <i>R</i> indexes [ <i>I</i> ≥ 2σ ( <i>I</i> )]	<i>R</i> <sub>1</sub> = 0.0440, <i>wR</i> <sub>2</sub> = 0.1190	<i>R</i> <sub>1</sub> = 0.0344, <i>wR</i> <sub>2</sub> = 0.0674
Final <i>R</i> indexes [all data]	<i>R</i> <sub>1</sub> = 0.0593, <i>wR</i> <sub>2</sub> = 0.1281	<i>R</i> <sub>1</sub> = 0.0444, <i>wR</i> <sub>2</sub> = 0.0699
Largest diff. peak/hole (e Å <sup>-3</sup> )	1.75/-1.11	0.49/-0.29

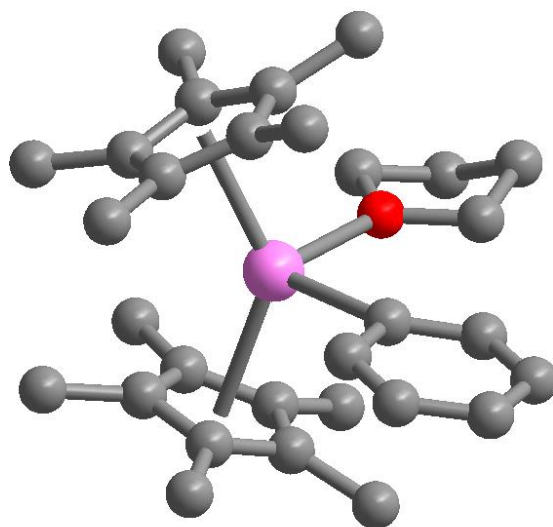


**Figure S1.** Structure of  $[\text{Cp}^*_2\text{Y}_2\text{Bi}_6]^{2-}$  in a crystal of **1**, with thermal ellipsoids drawn at 50% probability levels, shown in three different orientations. Pink, purple, and grey spheres represent Y, Bi, and C atoms, respectively. Hydrogen atoms and the  $[\text{K}(\text{THF})_4]^+$  cations have been removed for clarity.

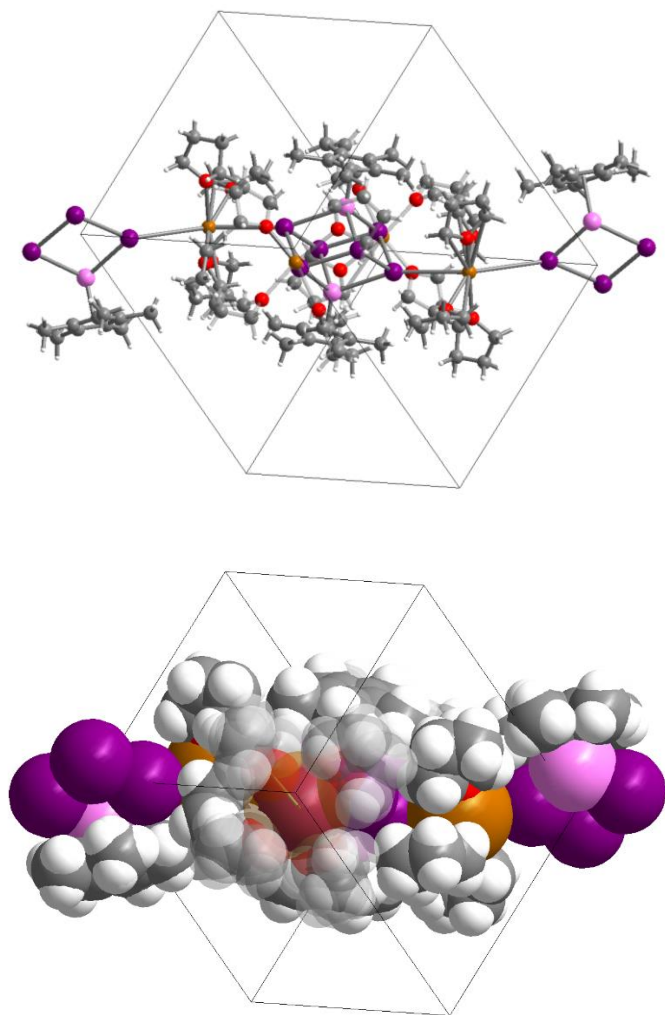


**Figure S2.** Space filling model of  $[\text{Cp}^*_2\text{Y}_2\text{Bi}_6]^{2-}$  in a crystal of **1**. Pink, purple, grey, and white spheres represent Y, Bi, C, and H atoms, respectively. The  $[\text{K}(\text{THF})_4]^+$  cations have been omitted for clarity.



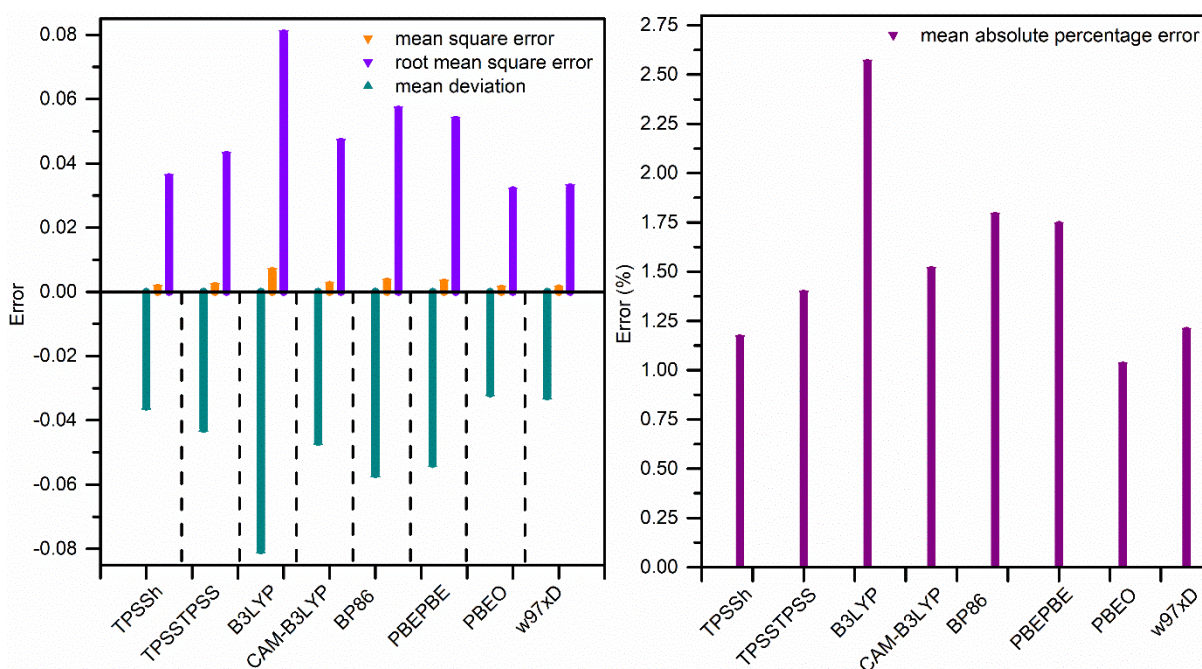


**Figure S3.** Structure of Cp\*<sub>2</sub>YPh(THF), **2**. Pink, red, and grey spheres represent Y, O, and C atoms, respectively. The H atoms have been omitted for clarity.

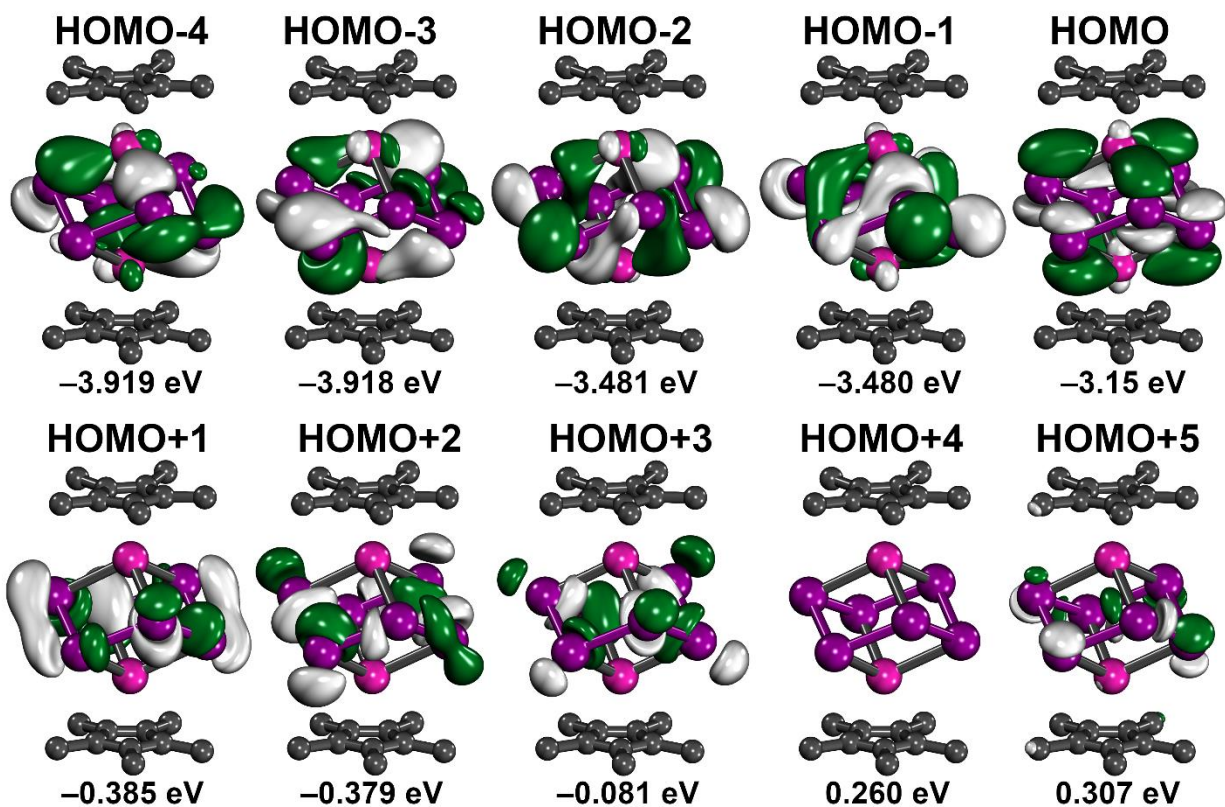


**Figure S4.** Crystal packing diagram of  $[\text{K}(\text{THF})_4][\text{Cp}^*_2\text{Y}_2\text{Bi}_6]$ , **1**, with the ball-and-stick (top) and space filling model (bottom) representations. Pink, purple, orange, red, grey, and white spheres represent Y, Bi, K, O, C, and H atoms, respectively.

### 1.3 DFT Calculations



**Figure S5.** Plots of the calculated mean deviation (MD), mean square error (MSE), root mean square error (RMSE) (left) and mean absolute percentage error (MAPE, right) obtained from the optimised molecular geometries of the  $[\text{Cp}^*_2\text{Y}_2\text{Bi}_6]^{2-}$  anion in comparison to its structural parameters obtained from single crystal X-ray diffraction analysis.



**Figure S6.** Plots of the calculated set of highest occupied molecular orbitals (HOMO-4 to HOMO+5) of the  $[\text{Cp}^*_2\text{Y}_2\text{Bi}_6]^{2-}$  anion, calculated on the rPBE0-GD3 6311+G\* (C,H)/ECP60MDF\_AVTZ (Y,Bi) level of theory. The isovalue was set to 0.03.

**Table S2.** Results of the hybridisation/polarisation analysis of NLMOs under consideration of a CPCM solvent model for THF, given as the % contributions of parent NBOs from rPBE0 calculations on the optimised structure of the  $[\text{Cp}^*_2\text{Y}_2\text{Bi}_6]^{2-}$  anion.

Orbital No.	Description	NLMO contributions				
		Occupancy	Bi	Y	Bi	Y
91	BD Bi <sup>1</sup> –Bi <sup>2</sup>	2.00	42.9	6.4	42.9	6.2
92	BD Bi <sup>1</sup> –Bi <sup>3</sup>	2.00	43.4	5.9	43.5	5.8
93	BD Bi <sup>1</sup> –Y <sup>4</sup>	2.00	77.8	18.1	-	-
94	BD Bi <sup>2</sup> –Y <sup>5</sup>	2.00	77.8	18.1	-	-
95	BD Bi <sup>2</sup> –Bi <sup>6</sup>	2.00	43.2	5.7	43.5	6.2
96	BD Bi <sup>3</sup> –Y <sup>5</sup>	2.00	77.9	18.1	-	-
97	BD Bi <sup>3</sup> –Bi <sup>7</sup>	2.00	43.4	6.2	43.2	5.9
98	BD Y <sup>4</sup> –Bi <sup>6</sup>	2.00	77.8	18.0	-	-
99	BD Y <sup>4</sup> –Bi <sup>7</sup>	2.00	77.9	18.1	-	-
100	BD Y <sup>5</sup> –Bi <sup>8</sup>	2.00	77.7	18.1	-	-
101	BD Bi <sup>6</sup> –Bi <sup>8</sup>	2.00	43.3	6.0	43.2	6.2
102	BD Bi <sup>7</sup> –Bi <sup>8</sup>	2.00	42.7	6.9	42.9	6.5

**Table S3.** Results of the hybridisation/polarisation analysis of NLMOs under consideration of a CPCM solvent model for THF, as the % orbital contributions from rPBE0 calculations on the optimised structure of the  $[\text{Cp}^*_2\text{Y}_2\text{Bi}_6]^{2-}$  anion.

Orbital No.	Description	Orbital contributions Atom 1 (%)			Orbital contributions Atom 2 (%)		
		s	p	d	s	p	d
91	BD Bi <sup>1</sup> –Bi <sup>2</sup>	3.9	95.5	0.6	4.1	95.2	0.6
92	BD Bi <sup>1</sup> –Bi <sup>3</sup>	3.5	95.9	0.7	3.5	95.8	0.7
93	BD Bi <sup>1</sup> –Y <sup>4</sup>	16.2	83.4	0.5	36.9	0.3	62.3
94	BD Bi <sup>2</sup> –Y <sup>5</sup>	15.9	83.6	0.5	35.3	0.3	63.9
95	BD Bi <sup>2</sup> –Bi <sup>6</sup>	3.3	96.0	0.6	3.8	95.5	0.6
96	BD Bi <sup>3</sup> –Y <sup>5</sup>	16.4	83.1	0.5	36.3	0.3	62.9
97	BD Bi <sup>3</sup> –Bi <sup>7</sup>	3.6	95.7	0.7	3.6	95.8	0.7
98	BD Y <sup>4</sup> –Bi <sup>6</sup>	35.1	0.3	64.0	15.8	83.7	0.5
99	BD Y <sup>4</sup> –Bi <sup>7</sup>	36.1	0.3	63.1	16.3	83.2	0.5
100	BD Y <sup>5</sup> –Bi <sup>8</sup>	36.2	0.3	63.0	15.8	83.7	0.5
101	BD Bi <sup>6</sup> –Bi <sup>8</sup>	3.5	95.8	0.7	3.3	96.0	0.7
102	BD Bi <sup>7</sup> –Bi <sup>8</sup>	3.7	95.6	0.6	4.0	95.3	0.6

**Table S4.** Results of the hybridisation/polarisation analysis of NLMOs under consideration of a CPCM solvent model for THF, given for the Bi lone electron pairs as the % orbital contributions as obtained from rPBE0 calculations on the optimised structure of the  $[\text{Cp}^*_2\text{Y}_2\text{Bi}_6]^{2-}$  anion.

NLMO No.	Description	NLMO contributions			
		Occupancy	s	p	d
83	LP1 Bi <sup>1</sup>	2.00	75.8	24.1	-
84	LP1 Bi <sup>2</sup>	2.00	76.0	23.9	-
85	LP1 Bi <sup>3</sup>	2.00	75.7	24.3	-
86	LP1 Bi <sup>6</sup>	2.00	76.0	23.9	-
87	LP1 Bi <sup>7</sup>	2.00	75.8	24.2	-
88	LP1 Bi <sup>8</sup>	2.00	76.1	23.9	-

**Table S5.** Results of the second order perturbation analysis of the optimised structure of the  $[\text{Cp}^*_2\text{Y}_2\text{Bi}_6]^{2-}$  anion under consideration of a CPCM solvent model from rPBE0. Only strongest interactions within the  $\text{Y}_2\text{Bi}_6$  are shown ( $> 2$  kcal/mol).

Donor	Acceptor	E (kcal/mol) NLMO
LP1 Bi <sup>1</sup>	LV1 Y <sup>4</sup>	2.07
LP1 Bi <sup>1</sup>	LV1 Y <sup>5</sup>	4.04
LP1 Bi <sup>1</sup>	LV2 Y <sup>5</sup>	5.42
LP1 Bi <sup>1</sup>	BD*1 Bi <sup>1</sup> -Y <sup>4</sup>	3.71
LP1 Bi <sup>1</sup>	BD*1 Bi <sup>2</sup> -Bi <sup>6</sup>	2.56
LP1 Bi <sup>1</sup>	BD*1 Bi <sup>3</sup> -Bi <sup>7</sup>	2.50
LP1 Bi <sup>2</sup>	LV1 Y <sup>4</sup>	6.47
LP1 Bi <sup>2</sup>	LV2 Y <sup>4</sup>	3.22
LP1 Bi <sup>2</sup>	BD*1 Bi <sup>1</sup> -Bi <sup>3</sup>	2.60
LP1 Bi <sup>2</sup>	BD*1 Bi <sup>2</sup> -Y <sup>5</sup>	4.09
LP1 Bi <sup>2</sup>	BD*1 Bi <sup>6</sup> -Bi <sup>8</sup>	2.63
LP1 Bi <sup>3</sup>	LV2 Y <sup>4</sup>	8.30
LP1 Bi <sup>3</sup>	LV1 Y <sup>5</sup>	2.49
LP1 Bi <sup>3</sup>	BD*1 Bi <sup>1</sup> -Bi <sup>2</sup>	2.55
LP1 Bi <sup>3</sup>	BD*1 Bi <sup>3</sup> -Y <sup>5</sup>	3.55
LP1 Bi <sup>3</sup>	BD*1 Bi <sup>7</sup> -Bi <sup>8</sup>	2.52
LP1 Bi <sup>6</sup>	LV2 Y <sup>4</sup>	2.02
LP1 Bi <sup>6</sup>	LV1 Y <sup>5</sup>	10.05
LP1 Bi <sup>6</sup>	BD*1 Bi <sup>1</sup> -Bi <sup>2</sup>	2.61
LP1 Bi <sup>6</sup>	BD*1 Y <sup>4</sup> -Bi <sup>6</sup>	4.27
LP1 Bi <sup>6</sup>	BD*1 Bi <sup>7</sup> -Bi <sup>8</sup>	2.64
LP1 Bi <sup>7</sup>	LV2 Y <sup>5</sup>	7.92
LP1 Bi <sup>7</sup>	BD*1 Bi <sup>1</sup> -Bi <sup>3</sup>	2.52
LP1 Bi <sup>7</sup>	BD*1 Y <sup>4</sup> -Bi <sup>7</sup>	3.71
LP1 Bi <sup>7</sup>	BD*1 Bi <sup>6</sup> -Bi <sup>8</sup>	2.59
LP1 Bi <sup>8</sup>	LV1 Y <sup>4</sup>	8.68
LP1 Bi <sup>8</sup>	LV2 Y <sup>4</sup>	2.07
LP1 Bi <sup>8</sup>	BD*1 Bi <sup>2</sup> -Bi <sup>6</sup>	2.62
LP1 Bi <sup>8</sup>	BD*1 Bi <sup>3</sup> -Bi <sup>7</sup>	2.54
LP1 Bi <sup>8</sup>	BD*1 Y <sup>5</sup> -Bi <sup>8</sup>	3.96
BD1 Bi <sup>1</sup> -Bi <sup>2</sup>	LV1 Y <sup>4</sup>	31.49

BD1 Bi <sup>1</sup> -Bi <sup>2</sup>	LV2 Y <sup>4</sup>	4.14
BD1 Bi <sup>1</sup> -Bi <sup>2</sup>	LV3 Y <sup>4</sup>	3.99
BD1 Bi <sup>1</sup> -Bi <sup>2</sup>	LV1 Y <sup>5</sup>	6.15
BD1 Bi <sup>1</sup> -Bi <sup>2</sup>	LV2 Y <sup>5</sup>	32.49
BD1 Bi <sup>1</sup> -Bi <sup>2</sup>	LV3 Y <sup>5</sup>	3.45
BD1 Bi <sup>1</sup> -Bi <sup>2</sup>	BD*1 Bi <sup>1</sup> -Y <sup>4</sup>	8.50
BD1 Bi <sup>1</sup> -Bi <sup>2</sup>	BD*1 Bi <sup>2</sup> -Y <sup>5</sup>	9.70
BD1 Bi <sup>1</sup> -Bi <sup>3</sup>	LV1 Y <sup>4</sup>	4.39
BD1 Bi <sup>1</sup> -Bi <sup>3</sup>	LV2 Y <sup>4</sup>	28.46
BD1 Bi <sup>1</sup> -Bi <sup>3</sup>	LV3 Y <sup>4</sup>	3.86
BD1 Bi <sup>1</sup> -Bi <sup>3</sup>	LV1 Y <sup>5</sup>	27.77
BD1 Bi <sup>1</sup> -Bi <sup>3</sup>	LV2 Y <sup>5</sup>	10.76
BD1 Bi <sup>1</sup> -Bi <sup>3</sup>	LV3 Y <sup>5</sup>	3.88
BD1 Bi <sup>1</sup> -Bi <sup>3</sup>	BD*1 Bi <sup>1</sup> -Y <sup>4</sup>	8.57
BD1 Bi <sup>1</sup> -Bi <sup>3</sup>	BD*1 Bi <sup>3</sup> -Y <sup>5</sup>	8.74
BD1 Bi <sup>1</sup> -Y <sup>4</sup>	LV2 Y <sup>5</sup>	2.26
BD1 Bi <sup>1</sup> -Y <sup>4</sup>	LV3 Y <sup>5</sup>	2.63
BD1 Bi <sup>2</sup> -Y <sup>5</sup>	LV1 Y <sup>4</sup>	2.15
BD1 Bi <sup>2</sup> -Y <sup>5</sup>	LV3 Y <sup>4</sup>	2.23
BD1 Bi <sup>2</sup> -Y <sup>5</sup>	BD*1 Bi <sup>3</sup> -Y <sup>5</sup>	2.09
BD1 Bi <sup>2</sup> -Y <sup>5</sup>	BD*1 Y <sup>5</sup> -Bi <sup>8</sup>	2.09
BD1 Bi <sup>2</sup> -Bi <sup>6</sup>	LV1 Y <sup>4</sup>	12.91
BD1 Bi <sup>2</sup> -Bi <sup>6</sup>	LV2 Y <sup>4</sup>	24.58
BD1 Bi <sup>2</sup> -Bi <sup>6</sup>	LV3 Y <sup>4</sup>	3.70
BD1 Bi <sup>2</sup> -Bi <sup>6</sup>	LV1 Y <sup>5</sup>	29.12
BD1 Bi <sup>2</sup> -Bi <sup>6</sup>	LV2 Y <sup>5</sup>	10.43
BD1 Bi <sup>2</sup> -Bi <sup>6</sup>	LV3 Y <sup>5</sup>	3.65
BD1 Bi <sup>2</sup> -Bi <sup>6</sup>	BD*1 Bi <sup>2</sup> -Y <sup>5</sup>	9.63
BD1 Bi <sup>2</sup> -Bi <sup>6</sup>	BD*1 Y <sup>4</sup> -Bi <sup>6</sup>	9.81
BD1 Bi <sup>3</sup> -Y <sup>5</sup>	LV2 Y <sup>4</sup>	2.80
BD1 Bi <sup>3</sup> -Y <sup>5</sup>	LV3 Y <sup>4</sup>	2.66
BD1 Bi <sup>3</sup> -Bi <sup>7</sup>	LV1 Y <sup>4</sup>	2.37
BD1 Bi <sup>3</sup> -Bi <sup>7</sup>	LV2 Y <sup>4</sup>	31.62
BD1 Bi <sup>3</sup> -Bi <sup>7</sup>	LV3 Y <sup>4</sup>	3.91
BD1 Bi <sup>3</sup> -Bi <sup>7</sup>	LV1 Y <sup>5</sup>	11.96



BD1 Bi <sup>3</sup> -Bi <sup>7</sup>	LV2 Y <sup>5</sup>	22.55
BD1 Bi <sup>3</sup> -Bi <sup>7</sup>	LV3 Y <sup>5</sup>	3.99
BD1 Bi <sup>3</sup> -Bi <sup>7</sup>	BD*1 Bi <sup>3</sup> -Y <sup>5</sup>	8.43
BD1 Bi <sup>3</sup> -Bi <sup>7</sup>	BD*1 Y <sup>4</sup> -Bi <sup>7</sup>	8.75
BD1 Y <sup>4</sup> -Bi <sup>6</sup>	LV1 Y <sup>5</sup>	3.51
BD1 Y <sup>4</sup> -Bi <sup>6</sup>	BD*1 Bi <sup>1</sup> -Y <sup>4</sup>	2.32
BD1 Y <sup>4</sup> -Bi <sup>6</sup>	BD*1 Y <sup>4</sup> -Bi <sup>7</sup>	2.37
BD1 Y <sup>4</sup> -Bi <sup>7</sup>	LV2 Y <sup>5</sup>	2.52
BD1 Y <sup>4</sup> -Bi <sup>7</sup>	LV3 Y <sup>5</sup>	2.28
BD1 Y <sup>5</sup> -Bi <sup>8</sup>	LV1 Y <sup>4</sup>	3.66
BD1 Y <sup>5</sup> -Bi <sup>8</sup>	LV3 Y <sup>4</sup>	2.42
BD1 Bi <sup>6</sup> -Bi <sup>8</sup>	LV1 Y <sup>4</sup>	22.08
BD1 Bi <sup>6</sup> -Bi <sup>8</sup>	LV2 Y <sup>4</sup>	19.13
BD1 Bi <sup>6</sup> -Bi <sup>8</sup>	LV3 Y <sup>4</sup>	3.39
BD1 Bi <sup>6</sup> -Bi <sup>8</sup>	LV1 Y <sup>5</sup>	38.56
BD1 Bi <sup>6</sup> -Bi <sup>8</sup>	LV3 Y <sup>5</sup>	3.67
BD1 Bi <sup>6</sup> -Bi <sup>8</sup>	BD*1 Y <sup>4</sup> -Bi <sup>6</sup>	10.06
BD1 Bi <sup>6</sup> -Bi <sup>8</sup>	BD*1 Y <sup>5</sup> -Bi <sup>8</sup>	9.19
BD1 Bi <sup>7</sup> -Bi <sup>8</sup>	LV1 Y <sup>4</sup>	39.35
BD1 Bi <sup>7</sup> -Bi <sup>8</sup>	LV3 Y <sup>4</sup>	3.77
BD1 Bi <sup>7</sup> -Bi <sup>8</sup>	LV2 Y <sup>5</sup>	34.02
BD1 Bi <sup>7</sup> -Bi <sup>8</sup>	LV3 Y <sup>5</sup>	3.59
BD1 Bi <sup>7</sup> -Bi <sup>8</sup>	BD*1 Y <sup>4</sup> -Bi <sup>7</sup>	8.94
BD1 Bi <sup>7</sup> -Bi <sup>8</sup>	BD*1 Y <sup>5</sup> -Bi <sup>8</sup>	9.05

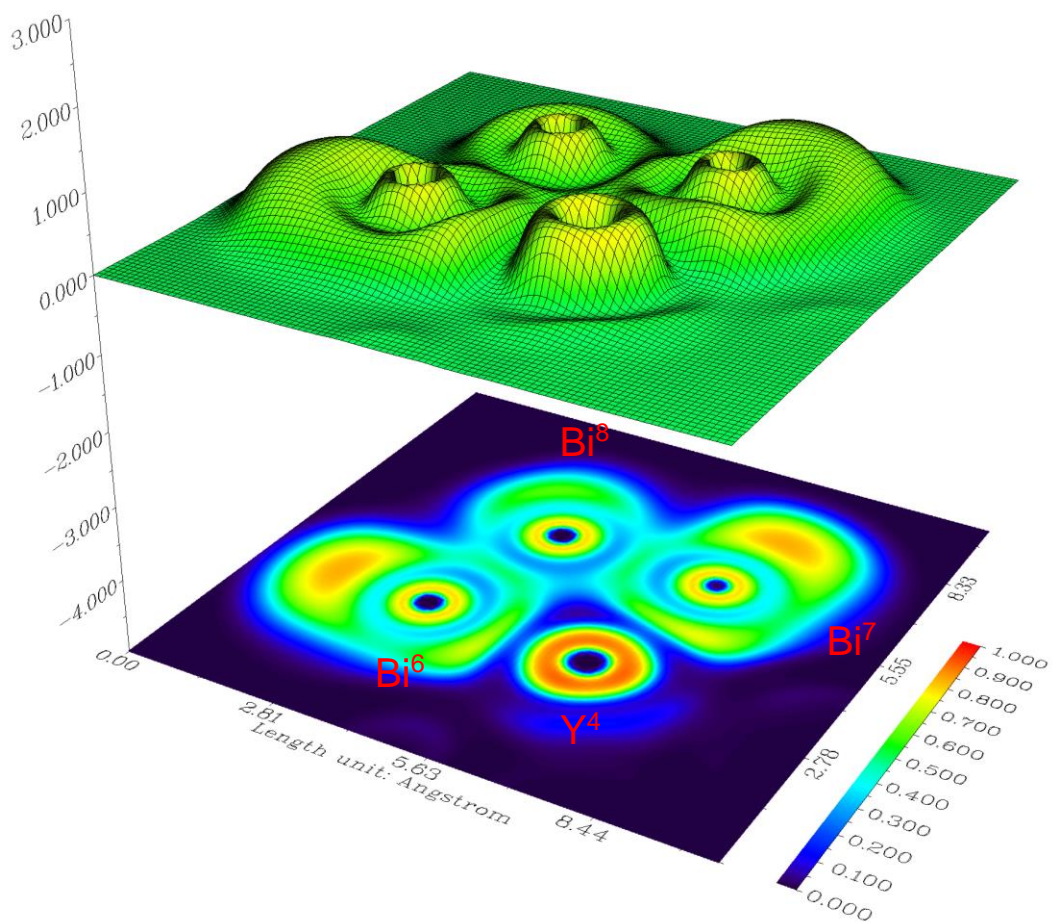
**Table S6.** Real space values of critical points as obtained from QTAIM analysis on the  $[\text{Cp}^*_2\text{Y}_2\text{Bi}_6]^{2-}$  anion along the  $\text{Y}^4$ ,  $\text{Bi}^6$ ,  $\text{Bi}^7$  and  $\text{Bi}^8$  plane.

Bond Critical Points (BCP, (3,-1))										
No	A-B	$\rho(r)$ (E-02)	$G(r)$ (E-02)	$K(r)$ (E-03)	$V(r)$ (E-02)	$H(r)$ (E-03)	$\nabla^2$ (E-02)	$H/\rho$ (E-01)	$\varepsilon(r)$ (E-02)	MBO
66	$\text{Bi}^2\text{-Bi}^6$	4.35	1.56	8.97	-2.46	-8.97	2.65	-2.06	1.55	0.973
69	$\text{Bi}^2\text{-Bi}^1$	4.36	1.56	9.00	-2.46	-9.00	2.65	-2.06	0.972	0.994
79	$\text{Bi}^2\text{-Y}^5$	3.38	1.44	6.00	-2.04	-6.00	3.37	-1.77	1.11	0.465
82	$\text{Bi}^6\text{-Y}^4$	3.41	1.46	6.09	-2.07	-6.09	3.40	-1.79	0.581	0.506
85	$\text{Bi}^1\text{-Y}^4$	3.36	1.43	5.95	-2.02	-5.95	3.33	-1.77	1.78	0.457
95	$\text{Bi}^6\text{-Bi}^8$	4.35	1.56	8.96	-2.46	-8.96	2.67	-2.06	1.43	0.969
105	$\text{Bi}^1\text{-Bi}^3$	4.35	1.55	8.95	-2.44	-8.95	2.62	-2.06	0.724	1.030
116	$\text{Y}^5\text{-Bi}^8$	3.37	1.44	5.96	-2.03	-5.96	3.36	-1.77	1.87	0.403
119	$\text{Y}^5\text{-Bi}^3$	3.39	1.44	6.05	-2.05	-6.05	3.35	-1.78	1.20	0.576
121	$\text{Y}^4\text{-Bi}^7$	3.40	1.45	6.05	-2.05	-6.05	3.37	-1.78	2.09	0.481
135	$\text{Bi}^3\text{-Bi}^7$	4.36	1.55	9.02	-2.45	-9.02	2.61	-2.07	0.457	1.051

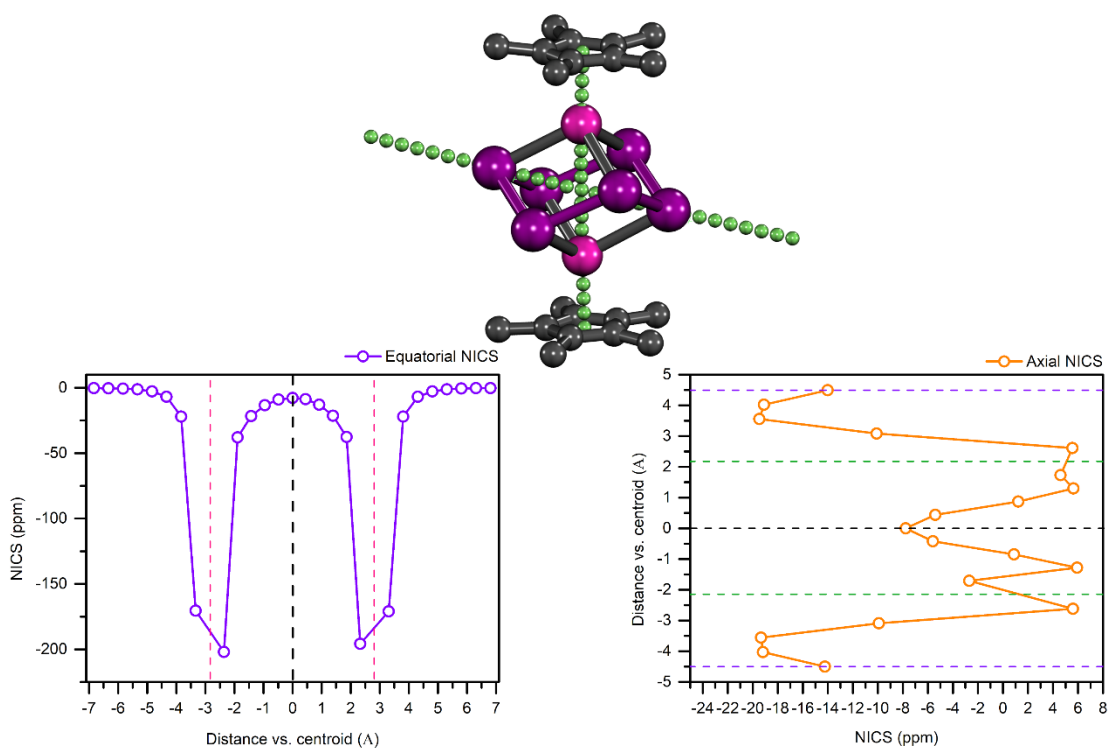
Ring Critical Points (RCP, (3,+1))											
	A-B	$\rho(r)$ (E-02)	$G(r)$ (E-03)	$K(r)$ (E-04)	$V(r)$ (E-03)	$H(r)$ (E-04)	$\nabla^2$ (E-02)	$H/\rho$ (E-02)	$\varepsilon(r)$	$\lambda_{\pi 3}$ (E-03)	SA (E-03)
75	$\text{Y}^4, \text{Bi}^1, \text{Bi}^2, \text{Bi}^6$	1.14	5.29	4.01	-5.69	-4.01	1.96	-3.53	-1.49	-4.70	7.92
88	$\text{Y}^5, \text{Bi}^2, \text{Bi}^6, \text{Bi}^8$	1.15	5.36	4.16	-5.78	-4.16	1.98	-3.61	-1.52	-4.80	8.01
94	$\text{Bi}^1, \text{Bi}^2, \text{Bi}^3, \text{Y}^5$	1.13	5.26	3.97	-5.66	-3.97	1.95	-3.51	-1.49	-4.65	7.81
107	$\text{Y}^4, \text{Bi}^6, \text{Bi}^7, \text{Bi}^8$	1.15	5.38	4.16	-5.79	-4.16	1.98	-3.61	-1.52	-4.83	7.45
113	$\text{Y}^4, \text{Bi}^1, \text{Bi}^3, \text{Bi}^7$	1.11	5.14	3.76	-5.52	-3.76	1.91	-3.39	-1.45	-4.50	7.97
125	$\text{Y}^5, \text{Bi}^3, \text{Bi}^7, \text{Bi}^8$	1.12	5.17	3.80	-5.55	-3.80	1.92	-3.40	-1.46	-4.54	7.84

Cage Critical Points (CCP, (3,+3))											
101	$\text{Bi}^1, \text{Bi}^2, \text{Bi}^3, \text{Bi}^6, \text{Bi}^7, \text{Bi}^8$	0.555	2.13	-0.0526	-2.13	0.0526	0.855	0.0948	-0.809	-	-

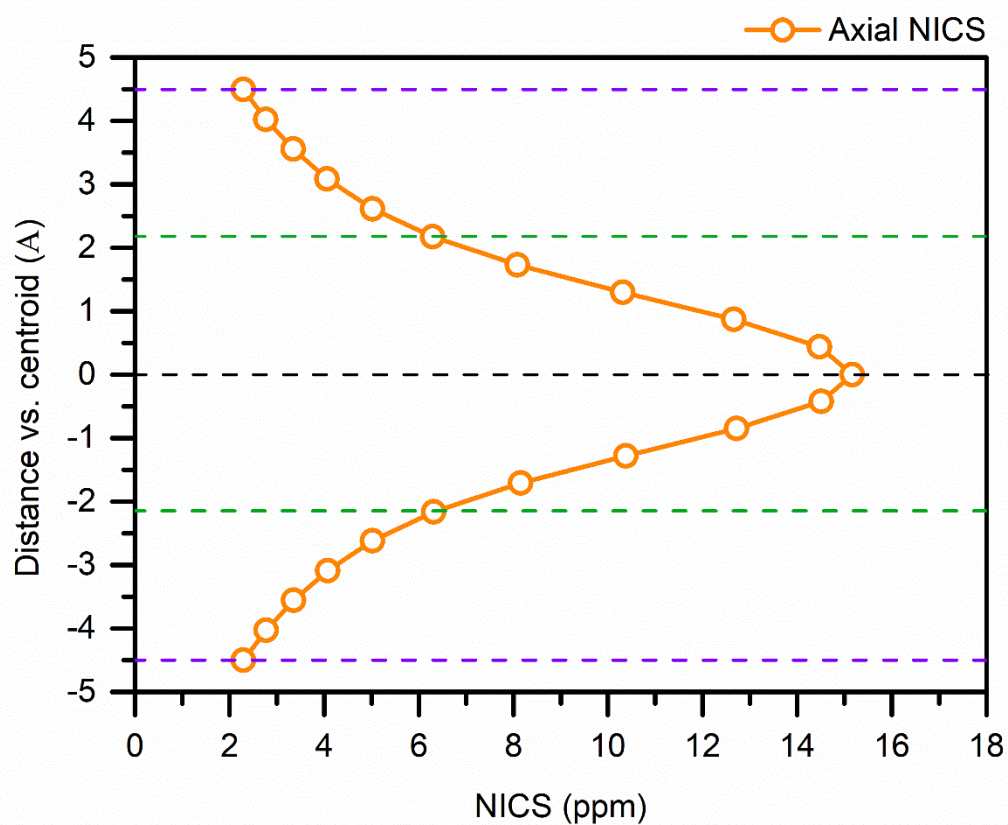
$\rho(r)$ : Density of all electrons;  $G(r)$ : Lagrangian kinetic energy;  $K(r)$ : Hamiltonian kinetic energy;  $V(r)$ : Potential energy;  $H(r)$ : Energy density;  $\nabla^2$ : Laplacian of electron density;  $\varepsilon$ : Ellipticity of electron density; MBO: Mayer Bond Order;  $\lambda_{\pi 3}$ : Curvature of the electron density perpendicular to RCP; SA: Shannon aromaticity index.



**Figure S7.** Plot of the electron localisation function (ELF) of the  $[\text{Cp}^*_2\text{Y}_2\text{Bi}_6]^{2-}$  anion along the plane spanned by the  $\text{Y}^4$ ,  $\text{Bi}^6$ ,  $\text{Bi}^7$  and  $\text{Bi}^8$  atoms. Values close to 1 refer to ideal localisation while values below 0.5 indicate strong delocalisation. Alternating local maxima and minima around the heavy atoms can be attributed to the electronic (shell) structure of these atoms, which is reliably reproduced through the ELF.<sup>42</sup> Most prominently, the local maxima on the Bi atoms facing outside the cluster core represent their lone electron pairs. Data of the C–H interaction occurring in this plane were omitted for clarity.



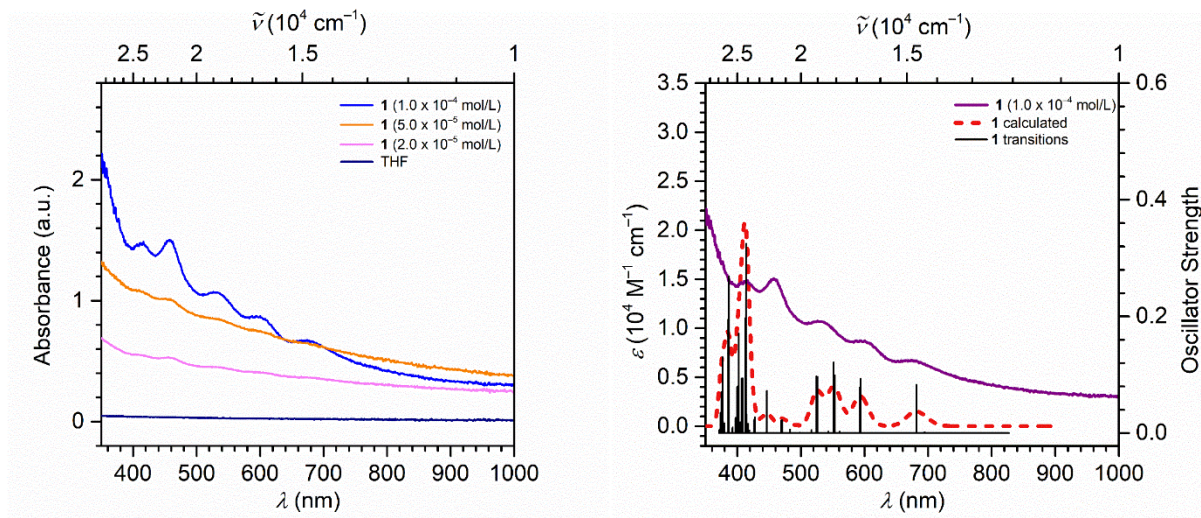
**Figure S8.** Top: Plot of the  $[\text{Cp}^*_2\text{Y}_2\text{Bi}_6]^{2-}$  anion with printed ghost atoms used for the calculation of the nuclear-independent chemical shift (NICS). Small green spheres, large pink and purple spheres represent ghost, Y and Bi atoms, respectively. Bottom: Distance-dependent plots of the calculated NICS values. Pink dotted lines represent positions of equatorial Bi atoms (left), green and purple dotted lines represent positions of Y atoms and Cp\* centroids (right), respectively. The more negative the NICS values, the stronger the deshielding of the respective ghost atoms.



**Figure S9.** Distance-dependent plots of the calculated NICS values for the  $\text{Bi}_6^{6-}$  core without capping  $(\text{Cp}^*\text{Y})^{2+}$  units. Green and purple dotted lines represent positions of Y atoms and  $\text{Cp}^*$  centroids. The more negative the NICS values, the stronger the deshielding of the respective ghost atoms.



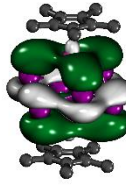
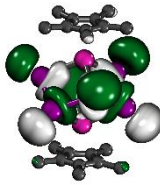
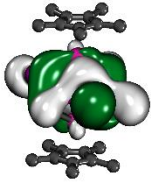
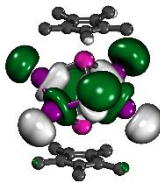
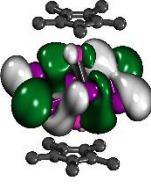
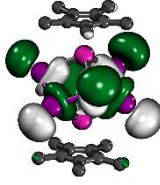
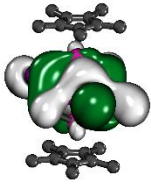
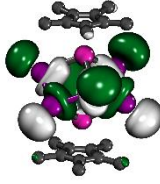
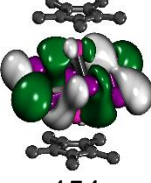
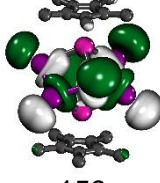
## 1.4 UV-Vis spectroscopy and TDDFT calculations

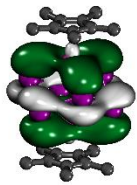
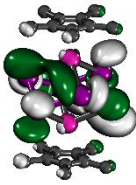
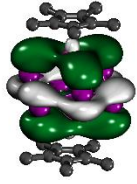
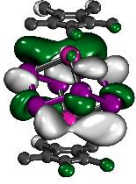
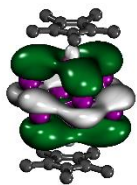
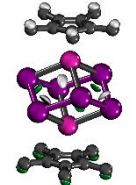
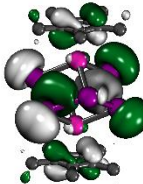
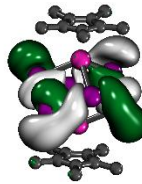
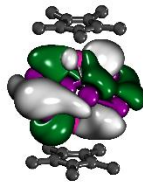



**Figure S10.** UV-Vis absorption spectra of **1** recorded at 100  $\mu\text{mol/L}$ , 50  $\mu\text{mol/L}$  and 20  $\mu\text{mol/L}$  concentrations in THF at room temperature (left). Comparison of the experimental UV-Vis spectrum of **1** (100  $\mu\text{mol/L}$ ) with Gaussian-broadened calculated spectrum (dashed red) and calculated transitions (black bars). Extinction coefficients represent y-dimension of experimental and calculated spectra, while the oscillator strength represents the y-dimension for the experimental and calculated spectra.

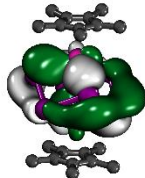

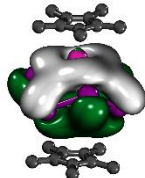
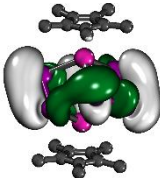
Several strong absorptions are predicted in the visible region that were deconvoluted to identify major transitions involved within these bands. The first calculated absorption is found at 681.2 nm and involves a HOMO  $\rightarrow$  HOMO+3 transition. The HOMO here can be described as a  $\text{Bi}_6^{6-}$   $\pi$ -type orbital. Towards smaller wavelengths, two sets of double absorptions are predicted at 593.8/592.6 nm and 553.3/551.4 nm, which comprise dominant HOMO-1  $\rightarrow$  HOMO+3 transitions for the higher wavelengths, and HOMO-2  $\rightarrow$  HOMO+3 transitions for the lower wavelengths. The occupied orbitals involved are primarily  $\sigma$ -bonding  $\text{Bi}_6^{6-}$  featuring considerable overlap with the yttrium atoms, while the virtual orbital HOMO+3 is composed of  $\text{Bi}_6^{6-}$   $\sigma^*$  orbitals. A third set of double excitations is predicted at 526.2/524.6 nm, comprising HOMO  $\rightarrow$  HOMO+5 and HOMO  $\rightarrow$  HOMO+6 transitions, where both virtual orbitals are best described as  $\text{Bi}_6^{6-}$   $\pi^*$  orbitals. At 446.4 nm, a HOMO  $\rightarrow$  HOMO+7 transition is calculated, where the virtual orbital exhibits  $\pi^*$  characteristics encompassing both the  $\text{Bi}_6^{6-}$  and  $\text{Cp}^*$  moieties.

**Table S7.** TDDFT-calculated transitions for the  $[\text{Cp}^*_2\text{Y}_2\text{Bi}_6]^{2-}$  anion on the 6311+G\*(C,H)/ECP\_AVTZ(Bi,Y) level using the PBE0 functional with dispersion correction GD3 and implicit solvent model CPCM for THF. The calculated excitation energies were empirically red shifted by 0.4 eV. HOMO: 156, LUMO: 157. Oscillator strength cutoff value: 0.07. Print threshold for individual transitions: 10%. Donor/acceptor orbitals are visualized for the dominant transitions with weights >40%. Isovalue for orbital depictions: 0.015.

$\lambda$ (nm)	$\tilde{\nu}$ ( $\text{cm}^{-1}$ )	Oscillator strength	Dominant Contributions (>10%)		Weight
			Occupied	Virtual	
681.2	14679.5	0.0829	 156	 159	89.8
593.8	16840.7	0.0930	 155	 159	50.7
			156	162	
592.6	16874.6	0.0789	153	157	10.5
			 154	 159	45.4
			156	161	
553.3	18072.1	0.0993	152	157	16.4
			152	158	12.1
			 155	 159	39.5
			156	162	
551.4	18136.2	0.1211	152	158	15.0
			 154	 159	44.2

			156	161	11.8
526.2	19004.3	0.0963	152	158	10.6
					49.7
524.6	19063.8	0.0975	156	161	
			153	158	10.5
					52.8
			156	162	
446.4	22400.9	0.0725			93.3
			156	163	
413.6	24177.0	0.3251	150	158	16.8
			152	162	10.9
			151	157	26.8
413.4	24190.5	0.2461	150	157	14.7
			151	158	19.1
412.7	24228.9	0.1548	151	157	11.3
			155	172	12.1
			156	168	10.9
412.6	24238.7	0.1974	151	158	18.3
					45.8
402.1	24871.5	0.1709	150	158	
			151	157	38.4
					44.7
386.6	25864.6	0.2686	153	160	
			153	164	13.4
			153	169	10.9



385.5	25940.1	0.1941	 152	 160	40.4
			152	164	10.7
			152	169	13.0
376.8	26542.7	0.1304	 149	 157	57.2
376.3	26572.0	0.0159	155	167	12.8
			155	168	19.6
375.4	26637.8	0.0709	149	158	29.6
			154	168	16.3

## 1.5 References

- 1 W. J. Evans, S. A. Kozimor, J. W. Ziller and N. Kaltsoyannis, *J. Am. Chem. Soc.*, 2004, **126**, 14533–14547.
- 2 D. E. Bergbreiter and J. M. Killough, *J. Am. Chem. Soc.*, 1978, **100**, 2126–2134.
- 3 B. J. Barker, H. L. Huffman and P. G. Sears, *J. Phys. Chem.*, 1974, **78**, 2689–2693.
- 4 S. Demir, J. M. Zadrozny, M. Nippe and J. R. Long, *J. Am. Chem. Soc.*, 2012, **134**, 18546–18549.
- 5 G. M. Sheldrick, *Acta Crystallogr. Sect. A*, 2015, **71**, 3–8.
- 6 G. M. Sheldrick, *Acta Crystallogr. Sect. C*, 2015, **71**, 3–8.
- 7 O. V Dolomanov, L. J. Bourhis, R. J. Gildea, J. A. K. Howard and H. Puschmann, *J. Appl. Crystallogr.*, 2009, **42**, 339–341.
- 8 D.J. Frisch, G.W. Trucks, H.B. Schlegel, G.E. Scuseria, M.A. Robb, J.R. Cheeseman, G. Scalmani, V. Barone, G.A. Petersson, H. Nakatsuji, X. Li, M. Caricato, A.V. Marenich, J. Bloino, B.G. Janesko, R. Gomperts, B. Mennucci, H.P. Hratchian, J.V. Ortiz, A.F. Izmaylov, J.L. Sonnenberg, D. Williams-Young, F. Ding, F. Lipparini, F. Egidi, J. Goings, B. Peng, A. Petrone, T. Henderson, D. Ranasinghe, V.G. Zakrzewski, J. Gao, N. Rega, G. Zheng, W. Liang, M. Hada, M. Ehara, K. Toyota, R. Fukuda, J. Hasegawa, M. Ishida, T. Nakajima, Y. Honda, O. Kitao, H. Nakai, T. Vreven, K. Throssell, J.A. Montgomery Jr, J.E. Peralta, F. Ogliaro, M.J. Bearpark, J.J. Heyd, E.N. Brothers, K.N. Kudin, V.N. Staroverov, T.A. Keith, R. Kobayashi, J. Normand, K. Raghavachari, A.P. Rendell, J.C. Burant, S.S. Iyengar, J. Tomasi, M. Cossi, J.M. Millam, M. Klene, C. Adamo, R. Cammi, J.W. Ochterski, R.L. Martin, K. Morokuma, O. Farkas, J.B. Foresman, D.J. Fox. Gaussian G16 B01. Gaussian, Inc.: Wallingford CT **2016**.
- 9 J. S. Binkley, J. A. Pople and W. J. Hehre, *J. Am. Chem. Soc.*, 1980, **102**, 939–947.
- 10 K. D. Dobbs and W. J. Hehre, *J. Comput. Chem.*, 1987, **8**, 880–893.
- 11 R. Ditchfield, W. J. Hehre and J. A. Pople, *J. Chem. Phys.*, 1971, **54**, 720–723.
- 12 T. Clark, J. Chandrasekhar, G. W. Spitznagel and P. V. R. Schleyer, *J. Comput. Chem.*, 1983, **4**, 294–301.
- 13 P. C. Hariharan and J. A. Pople, *Theor. Chim. Acta*, 1973, **28**, 213–222.
- 14 W. J. Hehre, K. Ditchfield and J. A. Pople, *J. Chem. Phys.*, 1972, **56**, 2257–2261.
- 15 D. Rappoport and F. Furche, *J. Chem. Phys.*, 2010, **133**, 134105-1–11.
- 16 K. A. Peterson, D. Figgen, M. Dolg and H. Stoll, *J. Chem. Phys.*, 2007, **126**, 124101.
- 17 K. A. Peterson, *J. Chem. Phys.*, 2003, **119**, 11099–11112.
- 18 J. Tao, J. P. Perdew, V. N. Staroverov and G. E. Scuseria, *Phys. Rev. Lett.*, 2003, **91**, 3–6.
- 19 V. N. Staroverov, G. E. Scuseria, J. Tao and J. P. Perdew, *J. Chem. Phys.*, 2004, **121**, 11507.
- 20 R. F. W. Bader, *Atoms in Molecules*, Clarendon Press, 1st edn., 1994.

- 21 S. H. Vosko, L. Wilk and M. Nusair, *Can. J. Phys.*, 1980, **58**, 1200–1211.
- 22 A. D. Becke, *J. Chem. Phys.*, 1993, **98**, 5648–5652.
- 23 P. J. Stephens, F. J. Devlin, C. F. Chabalowski and M. J. Frisch, *J. Phys. Chem.*, 1994, **98**, 11623–11627.
- 24 T. Yanai, D. P. Tew and N. C. Handy, *Chem. Phys. Lett.*, 2004, **393**, 51–57.
- 25 L. S. Kassel, *J. Chem. Phys.*, 1936, **4**, 276–282.
- 26 J. P. Perdew, *Phys. Rev. B*, 1986, **33**, 8822–8824.
- 27 J.-D. Chai and M. Head-Gordon, *Phys. Chem. Chem. Phys.*, 2008, **10**, 6615.
- 28 J. P. Perdew, K. Burke and M. Ernzerhof, *Phys. Rev. Lett.*, 1996, **77**, 3865–3868.
- 29 J. P. Perdew, K. Burke and M. Ernzerhof, *Phys. Rev. Lett.*, 1997, **78**, 1396–1396.
- 30 C. Adamo and V. Barone, *J. Chem. Phys.*, 1999, **110**, 6158–6170.
- 31 B. Metz, H. Stoll and M. Dolg, *J. Chem. Phys.*, 2000, **113**, 2563–2569.
- 32 Z. Chen, C. S. Wannere, C. Corminboeuf, R. Puchta and P. von R. Schleyer, *Chem. Rev.*, 2005, **105**, 3842–88.
- 33 S. Grimme, J. Antony, S. Ehrlich and H. Krieg, *J. Chem. Phys.*, 2010, **132**, 154104.
- 34 V. Barone and M. Cossi, *J. Phys. Chem. A*, 1998, **102**, 1995–2001.
- 35 M. Cossi, N. Rega, G. Scalmani and V. Barone, *J. Comput. Chem.*, 2003, **24**, 669–681.
- 36 A. E. Reed and F. Weinhold, *J. Chem. Phys.*, 1985, **83**, 1736–1740.
- 37 W. Moffitt, *J. Am. Chem. Soc.*, 1954, **76**, 3386–3392.
- 38 F. Cortés-Guzmán and R. F. W. Bader, *Coord. Chem. Rev.*, 2005, **249**, 633–662.
- 39 T. Lu and F. Chen, *J. Comput. Chem.*, 2012, **33**, 580–592.
- 40 X. Yang, C. P. Burns, M. Nippe and M. B. Hall, *Inorg. Chem.*, 2021, **60**, 9394–9401.
- 41 A. R. Eulenstein, Y. J. Franzke, N. Lichtenberger, R. J. Wilson, H. L. Deubner, F. Kraus, R. Clérac, F. Weigend and S. Dehnen, *Nat. Chem.*, 2021, **13**, 149–155.
- 42 A. D. Becke and K. E. Edgecombe, *J. Chem. Phys.*, 1990, **92**, 5397–5403.